Surface & Coatings Technology xxx (2009) xxx–xxx

Contents lists available at ScienceDirect

Surface & Coatings Technology

journal homepage: www.elsevier.com/locate/surfcoat

A study of structural and mechanical properties of sputter deposited nanocomposite Ti–Si–N thin films

Vipin Chawla [a,b], R. Jayaganthan [a,*], Ramesh Chandra [b]

[a] Department of Metallurgical and Materials Engineering & Centre of Nanotechnology, Indian Institute of Technology Roorkee, Roorkee-247667, India
[b] Nano Science Laboratory, Institute Instrumentation Centre, Indian Institute of Technology Roorkee, Roorkee-247667, India

ARTICLE INFO

Article history:
Received 5 March 2009
Accepted in revised form 1 October 2009
Available online xxxx

Keywords:
Ti–Si–N films
Sputtering
Microstructural characterization
Nanoindentation

ABSTRACT

Nanocomposite Ti–Si–N thin films were deposited on Si (100) and Stainless Steel (type 304) substrates by DC/RF magnetron sputtering. The effect of varying deposition parameters on the structural and mechanical properties of Ti–Si–N films was investigated by several characterization techniques such as XRD, FE-SEM, AFM, TEM, and Nanoindentor, respectively. XRD analysis of the thin films, with varying Si content revealed the (111) orientation up to 15.6 at.% Si content and thereafter the film become amorphous. The microstrain of the films decreases with increase in Si content as observed in the present work.
A reduction in grain size and the transformation of pyramidal shape of grain morphology into columnar and finally to amorphous structure occurs for the films deposited, with varying Si content, as evident from the microstructural analysis. The surface roughness of the Ti–Si–N films, calculated from its AFM images, decreases with varying Si content. The hardness and Young's modulus values of Ti–Si–N films were observed to increase up to 34 GPa and 275 GPa with 15.6 at.% Si content respectively but decreases afterwards with increase in Si content. The improvement in the hardness of the films (up to 34 GPa) is due to grain boundary hardening arising from the two phase structures consisting of nanocrystallites of TiN embedded in the amorphous matrix of Si_3N_4. With increasing Si contents beyond 15 at.%, hardness of the films decreases due to incomplete nitridation of Si owing to the deficit nitrogen source during deposition of the films.
© 2009 Published by Elsevier B.V.

1. Introduction

Ti–Si–N nanocomposite coatings have been shown immense interest in recent years due to its very high hardness, high wear resistance, and improved thermal stability as compared to TiN [1–8]. It was developed during the early 1980s [9,10] and the processing, structure, and property of nanocomposite coating were investigated in detail by Veprek et al. [11,12] and Prochazka et al. [13]. According to Veprek et al. [12], for the development of superhard and thermally stable nanocomposites, the formation of stable nanostructures by self-organisation is essential through the thermodynamically driven spinodal phase segregation. A high nitrogen activity (partial pressure $\geq 1 \times 10^{-3}$ mbar) and deposition temperature of 500–600 °C are required to realize the formation of thermally stable nanocomposites. The maximum hardness of nanocomposites is achieved when one monolayer of Si_3N_4 covers the surface of polar, hard transition metal nitride nanocrystals such as TiN, W_2N, etc. They reported that the factors such as formation of atomically sharp interfaces, impurities (oxygen contents) <0.2 at.%, and formation of tiny nanocrystals achieved through the deposition conditions favorable for thermodynamically driven phase segregation is essential for fabricating superhard nanocomposite coatings. Prochazka et al. [13] has synthesized nanocomposite TiN/Si_3N_4 with stable nanostructures by reactive magnetron sputtering and observed its high hardness value of ≥45 GPa. They reported that its high hardness value is due to the higher nitrogen pressure ≥0.002 mbar and high deposition temperature 550–630 °C used in the sputtering, which are favorable for the formation of stable nanostructures facilitated by phase segregation. An enhancement of hardness and refractory properties manifested in the nanocomposite Ti–Si–N was elucidated with the size effect of TiN nanocrystals embedded in the Si_3N_4 amorphous matrix, which act as an effective barrier for dislocation motion as reported in the literature [12]. Silicon content affects the physical properties of the films such as electrical resistivity, oxidation stability, and diffusivity. For example, the formation of amorphous Si_3N_4 thin films depends on Si content, which serves as an effective diffusion barrier than its polycrystalline films due to the absence of grain boundaries and extended defects. The Si content also reduces grain size of the TiN in nanocomposite Ti–Si–N thin films through the incorporation of amorphous SiN_x between grains. The absence of distinguishable crystalline phases in the nanocomposite films with fewer defects contribute to increased resistivity and barrier strength [14–24].

Kim et al. [25] have investigated Ti–Si–N hard coatings deposited on SKD11 steel substrates, in which TiN was deposited by the arc ion

* Corresponding author. Tel.: +91 1332 285869; fax: +91 1332 285243.
E-mail address: rjayafmt@iitr.ernet.in (R. Jayaganthan).

0257-8972/$ – see front matter © 2009 Published by Elsevier B.V.
doi:10.1016/j.surfcoat.2009.10.001

ARTICLE IN PRESS

plating (AIP) method while Si was incorporated into the films by sputtering technique. A maximum hardness of 45 GPa at Si content of 7.7 at.% was observed in the coatings. The size of TiN crystallites has reduced with increasing Si content and it was distributed with multiple orientations in the amorphous silicon nitride phase. Surface roughness of the Ti–Si–N coating also has decreased with increase of Si content. Mei et al. [26] have deposited Ti–Si–N nanocomposite films on high speed steel substrates by reactive magnetron sputtering. The microstructure and mechanical properties of films are affected by the varying percentage of Si contents. TiN nanocrystals with grain size of about 20 nm were formed in the Ti–Si–N films, with the Si contents ranging from 4.0 at.% to 9.0 at.%, and they were surrounded by Si_3N_4 interphase (1 nm thick) as observed in their work. The hardness (H) and elastic modulus (E) of films have increased with increasing Si contents and its maximum H and E values were 34.2 GPa and 398 GPa, respectively. With the further increase of Si content, the mechanical properties of films have reduced gradually and finally it reached lower than that of the TiN films. Jiang et al. [27] have deposited Ti–Si–N on Si (100) substrates at room temperature by reactive unbalanced DC-magnetron sputtering and characterized by XPS. It was shown that in Ti–Si–N films, the Si bonding was in the form of Si_3N_4 with low Si contents ($\leq$14 at.%), while it was in the form of both Si and Si_3N_4 at high Si contents ($\geq$18 at.%). Also, the grain size and surface roughness have decreased due to higher nucleation rate with increase in Si content.

Kim et al. [28] have investigated the DC reactive magnetron sputtered Ti–Si–N on SKD 11 steel substrate using HRTEM and XPS. They reported that the films consist of nano-sized TiN crystallites surrounded by an amorphous Si_3N_4 and crystallites of initially aligned microstructure are finer, randomly oriented, and fully penetrated by amorphous phase with increase in Si content; the films showed a nearly amorphous phase with higher Si content. The free Si was observed in the films, due to the deficit of the nitrogen source, when Si content was increased. The hardness value of approximately 38 GPa was obtained from the Ti–Si–N films with the Si content of 11 at.%, which showed a microstructure of fine TiN crystallites dispersed uniformly in an amorphous matrix. The hardness reduction with increase of Si content beyond a critical point was attributed to the thickening effect of amorphous Si_3N_4 rather than to the effect of free Si. Cairney et al. [29] have deposited Ti–Si–N coatings on Si(100) wafers by concurrent cathodic arc evaporation and magnetron sputtering. These Ti–Si–N coatings of varying Si contents were examined by cross sectional transmission electron microscopy and observed that the samples with low contents (0.8 and 1.5 at.% Si) exhibits a columnar grain structure, which is deformed by intergranular cracking and shear sliding at the grain boundaries, while samples with higher Si contents (9.5 and 12.5 at.% Si) consisted of TiN nanocrystals of 5 nm in size connected by an amorphous Si_3N_4 matrix. Xu et al. [30] have studied the reactive magnetron sputtered Ti–Si–N films on 321 steel substrates and substantiated the influence of Si into TiN, especially on microstructure and adhesion of the coating/substrate system. They have reported that the films consist of fine TiN crystals surrounded by an amorphous Si_3N_4 matrix and with increasing Si contents, the orientation of TiN crystals shifts from (111) to (200), the crystallite size significantly diminishes from 15 nm in a pure TiN thin films to 4.2 nm in the Ti–Si–N thin films containing 22.6 at.% Si. The addition of a certain amount of Si increases the hardness and Young's modulus of the coatings, reaching maximum values to 42 GPa and 320 GPa, respectively. The scratch tests indicated that the adhesive strength also improves with Si addition. Rebouta et al. [31] have deposited Ti–Si–N films on polished tool steel and high speed steel substrates (AISI M2) by reactive magnetron sputtering. The films revealed higher hardness values than those obtained for TiN. The hardness increases with small Si additions reaching the maximum values for Si content between 4 and 10 at.%. The denser sample (4.7 g/cm^3) with a Si content of approximately 2 at.% showed maximum E value of 462 GPa.

Although the Ti–Si–N films have been studied in detail, the mechanisms affecting the mechanical properties of the films vary with respect to the microstructures of films influenced by the sputtering parameters. Hence, it is very essential to investigate influence of microstructures, with varying deposition conditions, on the mechanical properties of nanocomposite Ti–Si–N films. Owing to this view, the present work has been focused to investigate the DC/RF magnetron sputtered nanocomposite Ti–Si–N thin films, with the chosen sputtering parameters and varying Si contents, in order to identify the factors facilitating the enhancement as well as reduction in hardness of the films. The films were characterized by XRD, FE-SEM, AFM and TEM to reveal the influence of processing parameters on microstructural characteristics. The Si contents in the Ti–Si–N thin films were analyzed by using Energy Dispersive Spectroscopy (EDS) attached with FE-SEM. The hardness and Young's modulus of the films were measured by nanoindentation technique and the mechanisms of hardening effect were explained using their microstructural and compositional features.

2. Experimental

2.1. Deposition of Ti–Si–N thin films

The Ti–Si–N films were deposited on Si (100) and Stainless Steel (type 304) substrates by Direct Current (DC)/Radio Frequency (RF) magnetron sputtering. DC magnetron sputtering is used for conducting targets such as metals or doped semiconductors but not for nonconducting targets (non metals or insulators) because of its nonconducting nature, positive ions would lead to a charging of the surface and subsequently to a shielding of the electric field. Subsequently, the ion current would die off. Therefore, RF magnetron sputtering (radio frequency of 13.56 MHz) is used for non-conducting and semiconductor targets in which an AC-voltage is applied to the target. In one phase, ions are accelerated towards the target surface to sputter material and in the other phase, charge neutrality is achieved.

The Si substrate was cleaned by first rinsing in Hydrofluoric acid to remove SiO_2 layer and then ultrasonic baths of acetone and methanol and finally dried under nitrogen gas. The Stainless Steel (type 304) substrate was first polished by using 1/0, 2/0, 3/0 and 4/0 grid SiC emery papers and then cloth polished up to mirror finish. The substrates were cleaned by ultrasonic baths to remove the SiC and dust particles. The sputtering targets were 99.99% pure Ti and Si disc (2″ diameter and 5 mm thick) fixed at an angle of 45° to each other and with the use of rotator, the substrate was rotated between Ti and Si targets continuously to perform a co-sputtering as shown in Fig. 1. DC sputtering and RF sputtering for Ti and Si targets were used, respectively, during deposition. The base pressure was better than 2×10^{-6}Torr and the sputtering was carried out in an $Ar+N_2$ atmosphere with the ratio 80:20. Reactive sputtering was used to deposit Ti–Si–N films in the present work. Before starting the deposition, the targets were pre-sputtered for 15 min with a shutter located in between the targets and the substrate. This shutter is

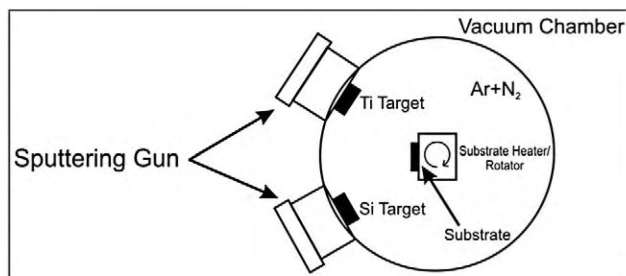

Fig. 1. Schematic diagram of experimental setup used for Ti–Si–N film deposition.

Please cite this article as: V. Chawla, et al., Surf. Coat. Technol. (2009), doi:10.1016/j.surfcoat.2009.10.001

ARTICLE IN PRESS

also used to control the deposition time. All the deposition was performed at a fixed substrate to target distance of 50 mm. The sputtering parameters for Ti–Si–N films with varying Si content are included in Table 1.

2.2. Characterization details

XRD (Bruker AXS, D8 Advance) measurements with using CuKα (λ = 1.54 Å) radiation to characterize the Ti–Si–N thin films. The excitation voltage and current were set to a 40 kV and 30 mA respectively, in the diffractometer. The grain size *t* of the Ti films was estimated from the Scherrer's formula [32], given as

$$t = \frac{0.9\lambda}{B\cos\theta} \quad (1)$$

where *B* (crystallite) is the corrected full-width at half maximum (FWHM) of a Bragg peak, λ is the wavelength of X-ray, and *θ* is the Bragg angle.

The texture coefficients of the Ti–Si–N films as a function of deposition time are calculated from their respective XRD peaks using the following formula [33];

$$Texture\,Coefficient(T) = \frac{I(hkl)}{[I(111) + I(200) + I(220)]} \quad (2)$$

where, *h*, *k*, *l* are planes and represents the (111), (200) or (220) orientations.

Cross sectional FE-SEM images were used to measure the thickness of Ti–Si–N films deposited on Si (100) substrate. FE-SEM (FEI, Quanta 200F) and TEM (FEI, Tecnai 20) were used to characterize the microstructures of the Ti–Si–N thin films at an acceleration voltage of 20 kV and 200 kV, respectively. The surface morphology (3D) of the Ti–Si–N films was characterized by AFM (NT-MDT, Ntegra) operated in semi contact (tapping) mode in order to calculate its surface roughness. The root-mean-square (RMS) roughness of the surface of the sample was calculated from AFM scan at five different spots for each sample.

2.3. Nanoindentation measurements

The hardness and elastic modulus of Ti–Si–N thin films were measured by using Hysitron nanoindentation instrument. In this nano hardness tester, an indenter tip with known geometry is driven into a specific site of the material to be tested by applying an increased normal load [34,35]. The load is increased and decreased in a linear fashion during the experiment. The diamond indenter is forced into the thin films being tested under constant load conditions. The loading profile during indentation testing followed linearly increasing with a hold time of 5 s at the peak load. The loads used were 10, 15, 20, 25 and 30 mN at loading rate 20.0 mN/min in the present work and the average hardness and Young's modulus value were calculated from the load–displacement curve obtained from the nanoindentation testing. Hardness values were consistent (δ = ± 1) from indent to indent and uniform over the range of indentation depth of 100–120 nm. The analysis of elastic modulus is based on the Oliver and Pharr Method [36].

Table 1
Sputtering parameters for Ti–Si–N films with variation of Si content.

Target	Ti (99.99% pure, 2 inch diameter and 5 mm thick) and Si (99.99% pure, 2 inch diameter and 5 mm thick)
Base pressure	2×10^{-6} Torr
Gas used	Ar: N_2 (80:20)
Sputtering (deposition) pressure	5 mTorr
Deposition time	90 min
Sputtering power for Ti target	150 W
Power density for Ti target	7.4 W/cm^2
Sputtering power for Si target	25–125 W (3.0–21.4 at.%)
Power density for Si target	1.23–6.17 W/cm^2
Substrate	Si (100) and Stainless Steel (type 304)
Substrate temperature	300 °C

3. Results and discussion

The XRD peaks for the nanocomposite Ti–Si–N films deposited at varying Si contents on Stainless Steel substrate are shown in Fig. 2(a). It is observed that with increasing Si content up to 12.8 at.%, the films exhibit (111) preferred orientation but with increase in Si contents above 12.8 at.%, intensity of (200) and (220) peaks grows up. However, no signals corresponding to crystalline Si_3N_4 and various phases of titanium silicide could be observed. It shows that Si was present in an amorphous phase of either Si_3N_4 or Si, which are in agreement with previous reports on Ti–Si–N nanocomposite films prepared by CVD and PVD [28,30]. With increase in Si contents of above 15.6 at.%, no peak could be observed in the XRD spectra, indicating that the TiN crystals become too tiny to detect or the whole coating becomes amorphous.

Epitaxial stabilization of cubic SiN_x in TiN/SiN_x multilayers was investigated in detail by both experimental and ab initio calculations by Soderberg et al. [37]. The transformation of crystalline (cubic) to amorphous layer of SiN_x occurs in the TiN/SiN_x multilayers when the thickness of SiN_x increases beyond 0.8 nm as reported in their work. It has been shown through ab initio calculations that the epitaxial

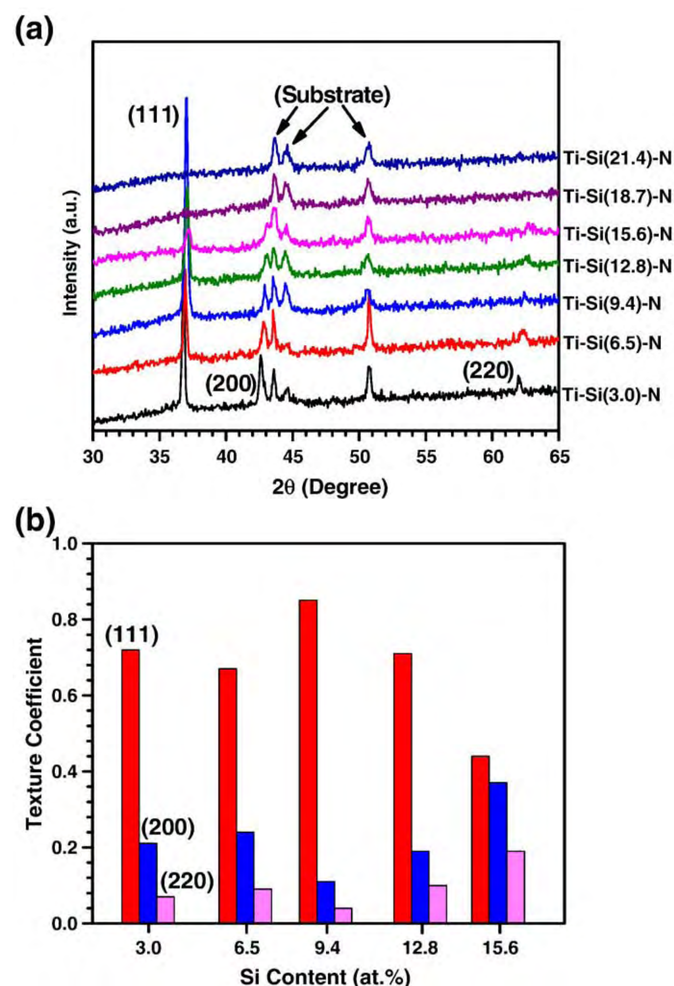

Fig. 2. (a) XRD peaks of Ti–Si–N films with variation of Si content and (b) texture coefficients of same films.

Please cite this article as: V. Chawla, et al., Surf. Coat. Technol. (2009), doi:10.1016/j.surfcoat.2009.10.001

ARTICLE IN PRESS

Table 2
Properties of Ti–Si–N films with variation of Si content.

Coating	Thickness (μm)	Interplanar spacing, (Å) (111) peak	Crystallite size (nm) (111) XRD	Lattice parameter, a (Å) (111) peak	Microstrain (111) peak	Average roughness (nm) AFM
Ti–Si (3.0 ± 0.4)–N	1.82	2.439	47.9 ± 1.7	4.224	0.823	67.7
Ti–Si (6.5 ± 0.7)–N	1.72	2.431	41.7 ± 1.9	4.211	0.492	48.2
Ti–Si (9.4 ± 0.9)–N	1.51	2.425	34.1 ± 2.2	4.200	0.239	39.7
Ti–Si (12.8 ± 1.1)–N	1.75	2.422	30.2 ± 2.4	4.195	0.119	36.3
Ti–Si (15.6 ± 1.3)–N	2.05	2.411	17.8 ± 3.1	4.176	−0.096	33.8
Ti–Si (18.7 ± 1.4)–N	1.72	–	–	–	–	29.4
Ti–Si (21.4 ± 1.5)–N	2.35	–	–	–	–	22.8

stabilization of cubic SiN_x occurs in the multilayers, only for the few monolayers of SiN_x, due to the minimization of interfacial energy at the early stages of layer nucleation and pseudomorphic forces present during subsequent coalescence and growth. The structural interfacial energy in addition to chemical interfacial energy contributes to the stabilization of amorphous structure of SiN_x if its thickness is higher than 0.8 nm.

The grain growth of TiN crystals is inhibited due to the presence of second phase particles causing Zener drag effect, which result in reduction of size of TiN crystals. The crystallite size of the thin film with 3.0 at.% Si, calculated from the X-ray peak broadening is 47.9 ± 1.7 nm and crystallite size decreases with increase in Si content and the size reduces to 17.8 ± 3.1 nm for 15.6 at.% Silicon. This indicates that TiN crystals become finer with the incorporation of the amorphous Si_3N_4 phase. It was also observed that with increase in Si contents; inter planar spacing, d decreases from 2.439 Å for 3.0 at.% Si to 2.411 Å for 15.6 at.% Si and thereafter, the films become amorphous with further increase in Si contents.

Fig. 2(b) shows the texture coefficients of the nanocomposite Ti–Si–N films deposited at varying Si content calculated from their respective XRD peaks by using the formula, as given in Eq. (2). From Fig. 2(b), it is observed that the texture coefficient of (111)

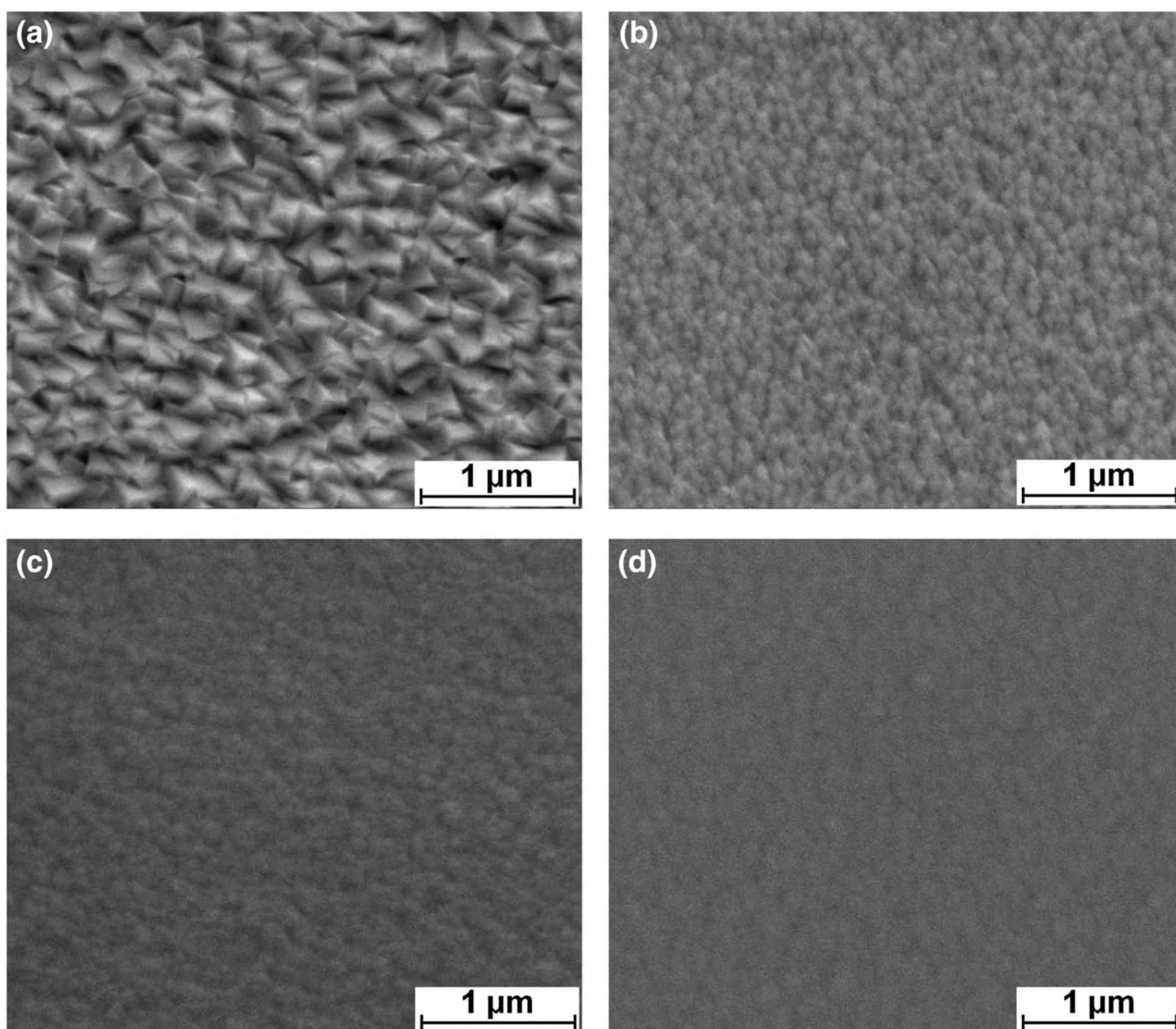

Fig. 3. FE-SEM images of Ti–Si–N films with variation of Si content (a) 3.0 at.%, (b) 9.4 at.%, (c) 15.6 at.% and (d) 21.4 at.%.

Please cite this article as: V. Chawla, et al., Surf. Coat. Technol. (2009), doi:10.1016/j.surfcoat.2009.10.001

ARTICLE IN PRESS

peak dominates till the Si content reaches 12.8 at.% and afterwards, other orientations such as (220) and (200) peaks develops.

The microstrain from (111) peak of Ti–Si–N films on Stainless Steel substrate were calculated by the following equation [38,39]:

$$\varepsilon = (a - a_o)/a_o \times 100 \quad (3)$$

where, a and a_o are the lattice parameters of the strained and unstrained Ti–Si–N films, respectively, which are calculated from XRD data [40]. The lattice parameter, a of Ti–Si–N films were calculated using the equation of cubic structure [32]:

$$\frac{1}{d^2} = \frac{(h^2 + k^2 + l^2)}{a^2} \quad (4)$$

where, d is the interplanar distance obtained from the position of the (111) peak using the Bragg condition, a is the lattice parameter and h, k and l are planes.

The lattice parameters of the films on Stainless Steel substrate for varying Si content are included in Table 2 and it is observed that with increase in Si contents, lattice parameter, a decreases. It is also evident that with increase in Si contents, microstrain, ε, decreases and the data of all Ti–Si–N films are included in Table 2.

The FE-SEM images of the Ti–Si–N films with increasing Si contents are shown in Fig. 3(a–d). It is observed that with increase in Si contents, grain size decreases and the initial pyramidal shape grains transform into columnar and finally to amorphous structure. The atomic percentage of Si in the Ti–Si–N films is calculated from the EDS results.

Fig. 4(a–d) shows the 3D AFM images of the Ti–Si–N films with increasing Si contents. It is evident from this figure that with increasing Si contents, grain size and surface roughness decreases, which could also be explained from the XRD results. With increase in Si contents, X-ray peak broadening is observed indicating the size reduction of TiN. The root mean square values of surface roughness with different Si contents on Stainless Steel (type 304) substrate calculated from the AFM images of the films are shown in Table 2.

Cross sectional FE-SEM images of varying Si content are shown in Fig. 5. It shows a columnar morphology and it becomes denser with increasing Si content (21.4 at.%). The thickness of Ti–Si–N measured from cross sectional FE-SEM images is included in Table 2.

TEM images in Bright field mode and selected area diffraction modes of Ti–Si–N films with varying Si contents are shown in Fig. 6(a–b). From Fig. 6(a), it is observed that the Ti–Si–N film with Si contents 6.5 at.% shows crystalline structure in Bright field mode with corresponding rings in selected area diffraction mode. On the other hand, in Fig. 6(b), with Si contents of 21.4 at.%, the diffraction patterns are diffused and bright field image revealed that the film consisted mainly of an amorphous phase. These results are in tandem with that of the XRD analysis.

Fig. 7(a) and (b) shows the AFM *in-situ* image of the indent on the sample which is obtained after the indentation and the influence of Si content on hardness and Young's modulus (E) of Ti–Si–N thin films, respectively. From Fig. 7(b), it is observed that the H and E values increases with increasing Si content and the films with 15.6 at.% Si contents show a maximum hardness and E values of 34 GPa and 275 GPa, respectively. However, these values drop when the Si content is increased beyond 15.6 at.%. An enhancement of

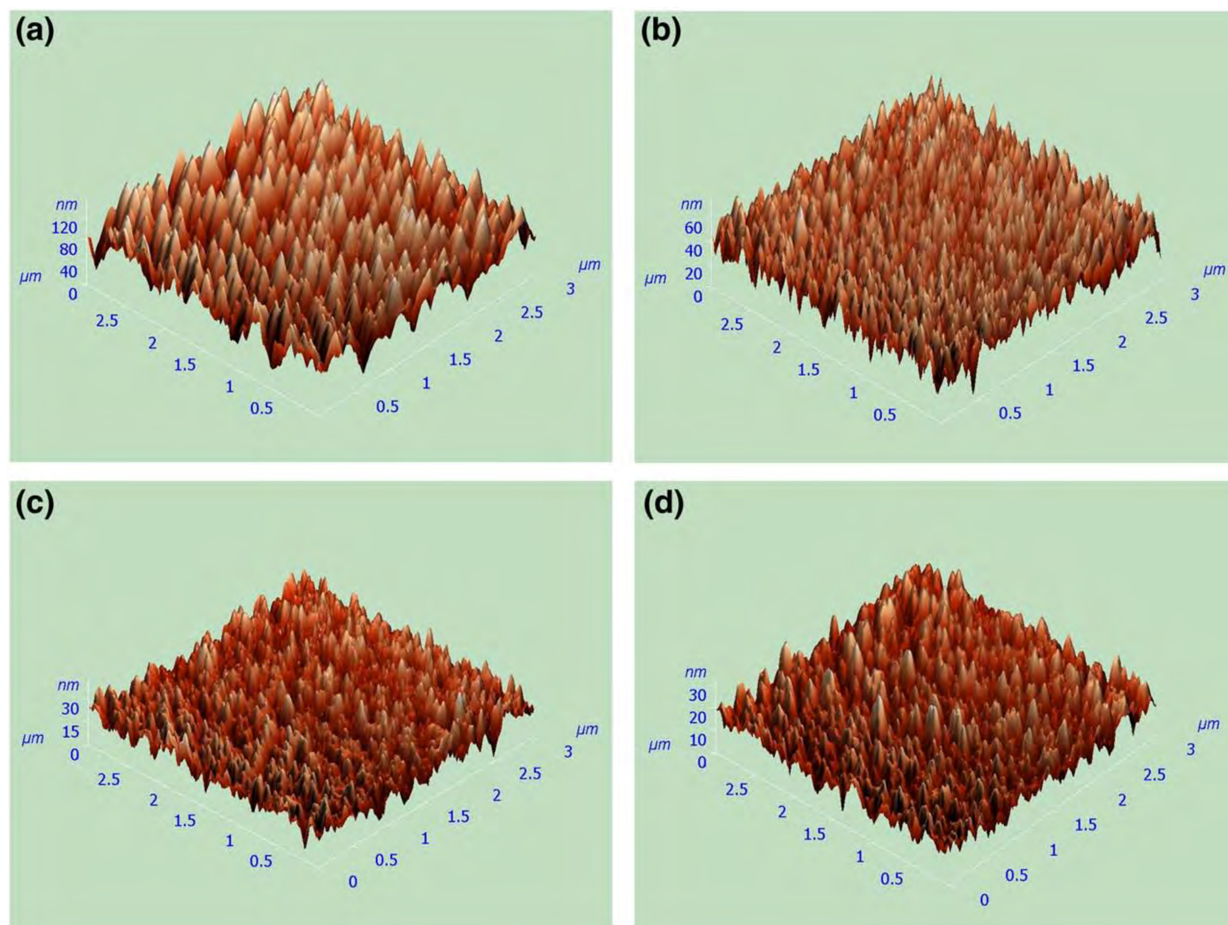

Fig. 4. 3D AFM images of Ti–Si–N films with variation of Si content (a) 3.0 at.%, (b) 9.4 at.%, (c) 15.6 at.% and (d) 21.4 at.%.

Please cite this article as: V. Chawla, et al., Surf. Coat. Technol. (2009), doi:10.1016/j.surfcoat.2009.10.001

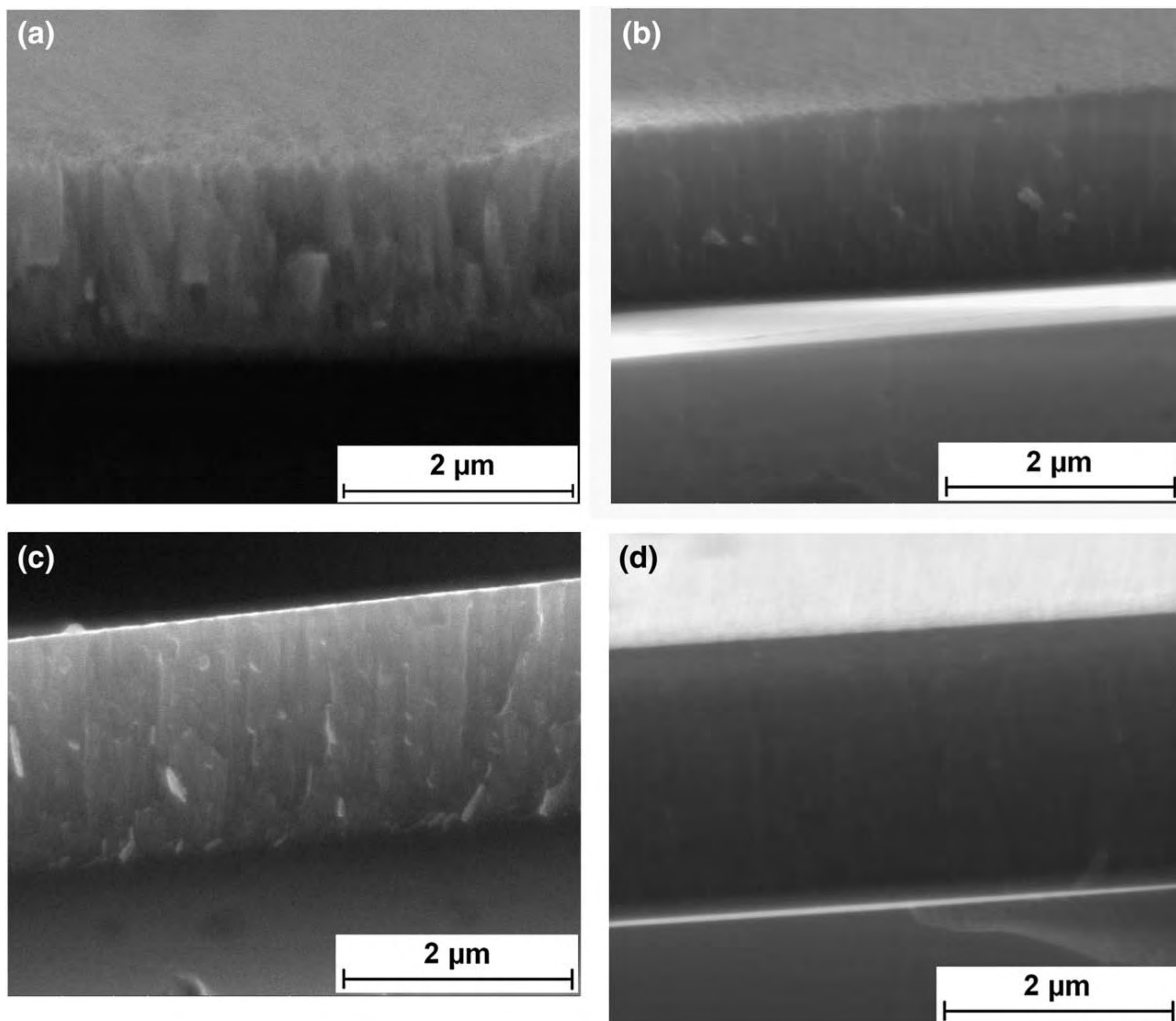

Fig. 5. Cross section FE-SEM images of Ti–Si–N films deposited on Si substrate at varying Si content (a) 3.0 at.%, (b) 9.4 at.%, (c) 15.6 at.% and (d) 21.4 at.%.

mechanical properties of Ti–Si–N films is considered to be due to its improved microstructure.

A possible phenomenological explanation to the observed hardness can be deduced from results of structural analyses and their comparison with existing concepts on nanocomposite mechanisms [41]. The formation of superhard nanocomposites requires 3–4 nm crystallite sizes with less than 1 nm thick separation in an amorphous matrix [42]. At these conditions, both dislocation formation and incoherence stress relaxation are suppressed, providing superhardness. The superhardness achieved in nc-TiN/a-Si_3N_4 nanocomposite is attributed to the strong nanostructure with an optimum thickness of one monolayer of the interfacial Si_3N_4 as reported by Veprek [43]. It is because of the pronounced quantum confinement, which contributes to strengthening, when the size of nanocrystal decreases to less than 4–5 nm. The difference in electronegativity leads to partial transfer of negative charge to silicon, which increases the bond strength. The decrease in hardness of the films beyond one monolayer thickness of the interface is due to the formation of misfit dislocation as explained in Veprek's work. He has further emphasized the influence of impurities at a level of >0.5 at.% of oxygen on substantial degradation of hardness of the films. The superhardening effect manifested in TiN/SiN_x multilayer is due to the epitaxial stabilization of cubic SiN_x, which occurs only for 1–2 monolayer thickness of the SiN_x (0.3–0.8 nm) [37]. A better lattice match (0.5%) of cubic SiN_x with TiN is found in this multilayer.

However, the Ti–Si–N films prepared in the present work exhibit large crystallite size, ~17–48 nm, which was sufficient for the formation of nanosized dislocations. This has limited the increase in hardness of the films in the present study. Nevertheless, it is observed that the improved hardness coincides with a reduction in grain size, which implies the presence of high volume fraction of grain boundaries. A two-phase structure consisting of nanocrystalline TiN surrounded by a matrix of amorphous Si_3N_4 could facilitate grain boundary hardening, contributing to the enhancement of hardness values. However, a reduction in hardness of the films occurs when the Si contents is increased (>15.6 at.%) during deposition of the films. It is due to the incomplete nitridation of Si, owing to the deficit of nitrogen source, leads to the presence of free Si in the films, which affects the properties of amorphous phase. Kim et al. [28] have also observed the presence of free Si in the DC reactive magnetron sputtered Ti–Si–N thin films, using HRTEM and XPS, when the Si content in the films is increased beyond 13.4 at.%.

4. Conclusions

The structural and mechanical properties of nanocomposite Ti–Si–N thin films deposited on Si (100) and Stainless Steel (type 304) substrates by DC/RF magnetron sputtering were investigated in the present work.

Please cite this article as: V. Chawla, et al., Surf. Coat. Technol. (2009), doi:10.1016/j.surfcoat.2009.10.001

ARTICLE IN PRESS

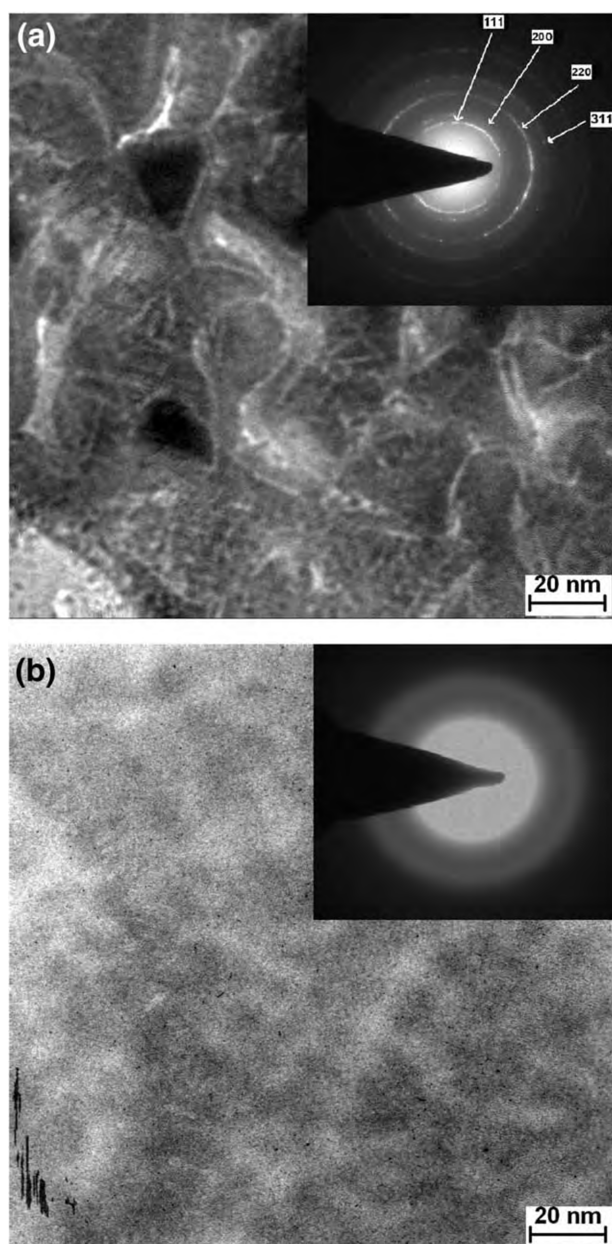

Fig. 6. Bright field image and SAD patterns by TEM of Ti–Si–N films deposited on Si substrate at varying Si content (a) at 6.5 at.% and (b) at 21.4 at.%.

XRD analysis of the thin films, with varying Si contents, revealed the (111) orientation up to 15.6 at.% Si content, beyond which the films become amorphous. The stabilization of amorphous structure, with the increase in thickness of SiN_x layer (>0.8 nm), is attributed to the chemical as well as the structural interfacial energy, which leads to the formation of misfit dislocations at the interface. The decrease in crystallite size and microstrain of the films is due to the formation of amorphous SiN_x layer with increasing Si contents as observed in the present work. Microstructural analysis of the films reveals a reduction in grain size and the transformation of pyramidal shape grains into columnar and finally to amorphous structure with varying Si contents.

The hardness and Young's modulus values of Ti–Si–N films have increased up to 34 GPa and 275 GPa, respectively, with 15.6 at.% Si contents. The high hardness of the films is governed by a two-phase structure consisting of nanocrystalline TiN and amorphous Si_3N_4, which facilitates the effective grain boundary hardening in the films. The reduction in hardness of the films with increasing Si addition

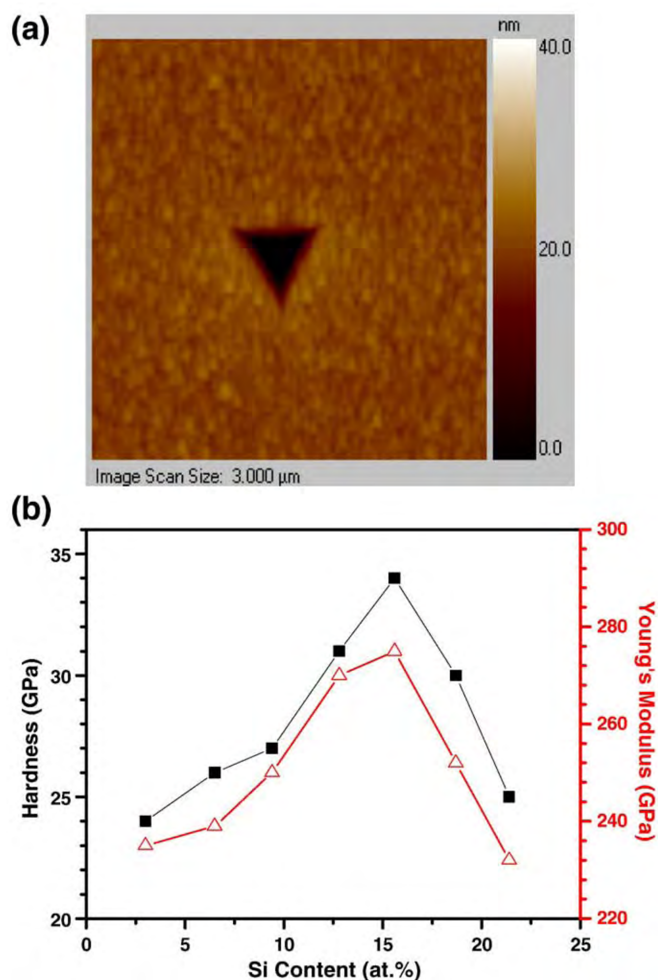

Fig. 7. (a) AFM *in-situ* image of the indent on the sample and (b) hardness and Young's modulus of Ti–Si–N films deposited with variation of Si content.

(>15.6 at.%) is due to the presence of free Si, which affects the properties of amorphous phase.

Acknowledgements

The author Dr. Ramesh Chandra would like to thank DST and DRDO, in India, for their financial support to this work and the other author Mr. Vipin Chawla is thankful to CSIR for an award of senior research fellowship.

References

[1] L. Shizhi, S. Yulong, P. Hongrui, Plasma. Chem. Plasma Process. 12 (1992) 287.
[2] M. Diserens, J. Patscheider, F. Levy, Surf. Coat. Technol. 108/109 (1998) 241.
[3] M. Diserens, J. Patscheider, F. Levy, Surf. Coat. Technol. 120/121 (1999) 158.
[4] S. Veprek, P. Nesladek, A. Niederhofer, F. Glatz, M. Jılek, M. Sima, Surf. Coat. Technol. 108/109 (1998) 138.
[5] S. Veprek, A. Niederhofer, K. Moto, T. Bolom, H.D. Mannling, P.M. Nesladek, G. Dollinger, A. Bergmaier, Surf. Coat. Technol. 133/134 (2000) 152.
[6] F. Vaz, L. Rebouta, P. Goudeau, J. Pacaud, H. Garem, J.P. Riviere, A. Cavaleiro, E. Alves, Surf. Coat. Technol. 133/134 (2000) 307.
[7] J. Patscheider, T. Zehnder, M. Diserens, Surf. Coat. Technol. 146/147 (2001) 201.
[8] P.J. Martin, A. Bendavid, Surf. Coat. Technol. 163/164 (2003) 245.
[9] T. Hirai, S. Hayashi, J. Mater. Sci. 18 (1983) 2401.
[10] J.S. Park, S.W. Kang, H. Kim, J. Vac. Sci. Technol. B 24 (2006) 1327.
[11] S. Veprek, S. Reiprich, Thin Solid Films 268 (1995) 64.
[12] S. Veprek, M.G.J. Veprek-Heijman, P. Karvankova, J. Prochazka, Thin Solid Films 476 (2005) 1.
[13] J. Prochazka, P. Karvankova, M.G.J.V. Heijman, S. Veprek, Mat. Sci. Eng. A 384 (2004) 102.

Please cite this article as: V. Chawla, et al., Surf. Coat. Technol. (2009), doi:10.1016/j.surfcoat.2009.10.001

ARTICLE IN PRESS

[14] K. J. Juo, J. D. Wiley, J. H. Perepesko, J. E. Nordman, D. B. Aaron, E. A. Dobisz, D. E. Madisen and R. E. Thomas, (Sandia National Laboratories, SAND82-0425) (1981) 137.
[15] B.L. Doyle, P.S. Peercy, J.D. Wiley, J.H. Perepesko, J.E. Nordman, J. Appl. Phys. 53 (1982) 6186.
[16] M.A. Nicolet, I. Suni, M. Finetti, Solid State Technol. 26 (1983) 129.
[17] M.A. Nicolet, Appl. Surf. Sci. 91 (1995) 269.
[18] X. Sun, J.S. Reid, E. Kolawa, M.A. Nicolet, J. Appl. Phys. 81 (1997) 656.
[19] X. Sun, J.S. Reid, E. Kolawa, M.A. Nicolet, R. Ruiz, J. Appl. Phys. 81 (1997) 664.
[20] X. Sun, E. Kolawa, S. Im, C. Garland, M.A. Nicolet, Appl. Phys. A Mater. 65 (1997) 43.
[21] T. Kacsich, M.A. Nicolet, Thin Solid Films 349 (1999) 1.
[22] T. Kacsich, S. Gasser, Y. Tsuji, A. Dommann, M.A. Nicolet, J. Appl. Phys. 85 (1999) 1871.
[23] T. Kacsich, S.M. Gasser, C. Garland, M.A. Nicolet, Surf. Coat. Technol. 124 (2000) 162.
[24] E. Varesi, G. Pavia, A. Zenkevich, Yu. Lebedinskii, P. Besana, A. Giussani, A. Modelli, J. Phys. Chem. Solids 68 (2007) 1046.
[25] K.H. Kim, S.R. Choi, S.Y. Yoon, Surf. Coat. Technol. 161 (2002) 243.
[26] F. Mei, N. Shao, X. Hu, G. Li, M. Gu, Mater. Lett. 59 (2005) 2442.
[27] N. Jiang, Y.G. Shen, Y.-W. Mai, T. Chan, S.C. Tung, Mater. Sci. Eng. B 106 (2004) 163.
[28] S.H. Kim, J.K. Kim, K.H. Kim, Thin Solid Films 420/421 (2002) 360.
[29] J.M. Cairney, M.J. Hoffman, P.R. Munroe, P.J. Martin, A. Bendavi, Thin Solid Films 479 (2005) 193.
[30] Y. Xu, L. Li, X. Cai, P.K. Chu, Surf. Coat. Technol. 201 (2007) 6824.
[31] L. Rebouta, C.J. Tavares, R. Aimo, Z. Wang, K. Pischow, E. Alves, T.C. Rojas, J.A. Odriozola, Surf. Coat. Technol. 133/134 (2000) 234.
[32] B.D. Cullity, S.R. Stock, Elements of X-ray diffraction, third ed. Prentice Hall, New York, 2001.
[33] J.H. Huang, K.W. Lau, G.P. Yu, Surf. Coat. Technol. 191 (2005) 17.
[34] A.C. Fischer- Cripps, Nanoindentation, Mechanical Engineering Series, Springer-Verlag, New York, 2001.
[35] J.L. Hay, G.M. Pharr, ASM Handbook, Materials Testing and Evaluation, vol. 8, 2000, p. 232.
[36] W.C. Oliver, G.M. Pharr, J. Mater. Res. 7 (1992) 1564.
[37] H. Soderberg, M. Oden, T. Larsson, L. Hultman, J.M. Molina-Aldareguia, Appl. Phys. Lett. 88 (1–3) (2006) 191902.
[38] H.C. Ong, A.X.E. Zhu, G.T. Du, Appl. Phys. Lett. 80 (2002) 941.
[39] P. Singh, D. Kaur, J. Appl. Phys. 103 (2008) 1 043507.
[40] F. Vaz, L. Rebouta, R.M.C. Silva, M.F. Silva, J.C. Soares, Vacuum 52 (1999) 209.
[41] S. Veprek, S. Reiprich, L. Shizhi, Appl. Phys. Lett. 66 (1995) 2640.
[42] S. Veprek, J. Vac. Sci. Technol. A 17 (1999) 2401.
[43] S. Veprek, High Pressure Res. 26 (2006) 119.

Please cite this article as: V. Chawla, et al., Surf. Coat. Technol. (2009), doi:10.1016/j.surfcoat.2009.10.001